Ionics (2018) 24:2689–2696
https://doi.org/10.1007/s11581-017-2412-3

ORIGINAL PAPER

Construction of 3D polypyrrole/CoS/graphene composite electrode with enhanced pseudocapacitive performance

Yun Zhang [1,2] · Jianqiang Zhang [3] · Liu Wan [2] · Yuhong Ma [2] · Tongxiang Liang [4] · Xiaocheng Li [1,2] · Lingbin Kong [1]

Received: 19 July 2017 / Revised: 29 November 2017 / Accepted: 19 December 2017 / Published online: 4 January 2018

Abstract

Herein, 3D graphene/nickel foam (GE/NF) composite matrix was successfully fabricated by using NF as template through a self-catalytic thermal chemical vapor deposition process. By using the prepared GE/NF as substrate, CoS nanosheets were deposited via a facial one-step electrochemical deposition method. Owing to the advantage of GE in boosting the electrical contact between the electroactive host material and current collector, the as-prepared 3D CoS/GE/NF electrode demonstrated a superior capacitance value of 2308 F g^{-1} at 1 A g^{-1} and a high rate capability of 70.49% at 20 A g^{-1}. After depositing the polypyrrole (PPY) film on 3D CoS/GE/NF electrode, the electrochemical performance of CoS was further greatly improved and delivered an extremely high capacitance value of 3450 F g^{-1} at 1 A g^{-1}, with good rate capability (62.61% at 20 A g^{-1}) and improved cycling stability. The enhanced electrochemical performance of PPY/CoS/GE/NF electrode is closely related to the advantage of PPY film in increasing the electrical conductivity and reinforcing the integrity of electrode.

Keywords Pseudocapacitor · Cobalt sulfide · Graphene · Polypyrrole

Introduction

Efficient harvesting and utilization of renewable/alternative energy resources, such as wind, solar energy, and geothermal energy, is considered to be an appealing method to alleviate the rapid consumption of fossil fuel and thus induced serious environmental pollution [1]. However, these energy resources usually work unstably and strongly depend on natural conditions [2]. To make these energy resources be stably outputted, high-performance energy storage systems are therefore needed to partake in the power fluctuation smoothing, peak shaving, and valley filling. Among all energy storage systems, pseudocapacitors (PCs) have been regarded as one of promising candidates due to their high power density, fast charging/discharging rate, super-long lifespan, and excellent cycling stability [3–5]. In general, the electrode materials of PCs mainly include electroactive conducting polymers, and transition metal oxide/hydroxide (TMO/TMHO). Among them, the TMO/TMHO-based pseudocapacitors are principally dominated by the faradaic redox reaction and have proved to possess higher capacitance than carbon-based EDLCs. Driven by their high theoretic capacitance, various TMO/TMHO, including RuO_2 [6], MnO_2 [7], NiO [8], $Ni(OH)_2$ [9], Co_3O_4 [10], Fe_2O_3 [11], and their binary components, such as NiCo layered double hydroxide (LDH) [12], NiAl LDH [13], $NiCo_2O_4$ [14], and $Ni(OH)_2$/NiO [15], have been successfully constructed on nickel foam (NF) or carbon-based current collector. Since the faradaic occurred both on the electrode surface and also in the bulk of active material, the as-prepared TMO/TMHO-based pseudocapacitive materials delivered the acceptable specific capacitance. As evinced by a large number of research articles and technical reports, these pseudocapacitive TMO/TMHO materials still suffer from their low intrinsic electrical conductivity, which together with ion diffusion rate, determines the electrochemical

✉ Xiaocheng Li
xiaocheng@licp.cas.cn

1 State Key Laboratory of Advanced Processing and Recycling of Non-ferrous Metal, Lanzhou University of Technology, Lanzhou 730050, People's Republic of China

2 Laboratory of Clean Energy Chemistry and Materials, Lanzhou Institute of Chemical Physics, Chinese Academy of Sciences, Lanzhou 730000, People's Republic of China

3 School of Petrochemical Engineering, Lanzhou University of Technology, Lanzhou 730050, People's Republic of China

4 School of Material Science and Engineering, Jiangxi University of Science and Technology, Ganzhou 341000, People's Republic of China

performance of active material [16, 17]. To develop high-energy-density pseudocapacitor device, it is urgent to explore new positive pseudocapacitive material with high electrical conductivity, high theoretic capacitance value, and excellent cycling stability.

Recently, transition metal sulfides (TMS) have attracted much interest due to their high electrical conductivity, low-cost, environmental benignity, and natural abundance [18]. It has been established that the TMS exhibit the typical metal characteristics rather than the semiconductor, much different from that of corresponding TMO or TMHO compound. As an important family of TMS, the electrochemical performance of CoS received special attention, owing to their rich redox couples (Co^{2+}/Co^{3+} and Co^{3+}/Co^{4+}), variety morphologies, and ultra-high theoretic capacitance value [19]. According to eq. $C=\alpha\times F/(\Delta V\times M)$ (where α is the moles of charge per mole of CoS, F is Faraday's constant, ΔV is the potential window, and M is the mole mass of CoS), the theoretic capacitance value of stoichiometric CoS is calculated to be as high as 4241 F g^{-1} on the premise that the Co^{2+} was finally converted to Co^{4+}. Triggered by these special physical and chemical features, various CoS materials were prepared and their electrochemical properties were evaluated. For example, amorphous CoS polyhedral nanocage, which prepared by utilizing zeolitic imidazolate framework-67 nanocrystals as templates, can deliver a high specific capacitance of 1475 F g^{-1} at a current density of 1 A g^{-1} [20]. Lately, cathodic deposited cobalt sulfide nanosheets on NF demonstrate a high capacitance of 1471 F g^{-1} [21]. The achieved capacitance values of the cobalt sulfide-based electrode are much higher than that of cobalt oxide (CoO or Co_3O_4), confirming the improvement of capacitance due to sulfuration [22]. Despite the remarkable progress, these attempts still failed to further improve the capacitive performance of cobalt sulfides due to the inferior interfacial contact between the cobalt sulfides and the native oxide layer on nickel foam current collector. Moreover, currently, the electrochemical performance of TMS materials still suffer from the serious capacitance deterioration associating with the repeated lattice expansion/shrink and attenuation of active material during the charging/discharging process [23–25]. Therefore, a highly conductive but chemical-inert current collector as well as a highly conductive protecting film is needed to optimize the electrical interfacial contact and meanwhile consolidate the nanostructure of cobalt sulfide.

In light of these considerations, herein, we report a two-step process for fabricating the 3D porous polypyrrole/CoS/graphene (PPY/CoS/GE) composite electrode. Thanks for the highly conductive graphene film in reducing the interfacial electrical resistance between the CoS and current collector, as well as the highly conductive PPY film in consolidating the configuration of CoS nanosheets, the as-prepared 3D PPY/CoS/GE composite electrode showed greatly improved capacitance and cycling stability as compared with those of CoS/GE/NF and CoS/NF electrodes.

Experimental section

Deposition of 3D graphene on NF

Deposition of 3D graphene layer on NF substrate was realized through a self-catalytic thermal chemical vapor deposition (TCVD) strategy, as described elsewhere [26]. Prior to deposition, NF substrates ($1 \times 1 \times 0.1$ cm^3) were successively rinsed in 3 M HCl, deionized water, and absolute ethanol in an ultrasonic bath for 15 min. Then, the cleaned NFs were introduced into the center of the quartz tube of a TCVD system and heated up to 1000 °C at a ramp rate of 10 °C/min under Ar/H_2 atmosphere (Ar: H_2 = 200:20 sccm), and annealed for 5 min to reduce the native oxide layer on NF surface. Subsequently, absolute ethanol was introduced and used as carbon source to grow graphene by using Ar/H_2 as a carrier gas. After desired growth time, the samples were rapidly cooled down to room temperature under Ar/H_2 flow and finally taken out for following experiments.

Fabrication of 3D CoS/GE/NF electrode

Deposition of cobalt sulfide on NF and NF/GE substrates was carried out on a commercial CHI660E electrochemical working station (Chenhua, Shanghai) within a deposition bath containing 5 mM of $CoCl_2{\cdot}6H_2O$ and 0.75 M of thiourea. The pH value of the electrolyte was adjusted to 6 using a small amount of diluted NH_4OH aqueous solution. The electrochemical deposition was performed by using cyclic voltammetry (CV) in a potential interval from -1.24 to 0.16 V (vs. SCE) with a scan rate of 5 mV s^{-1} for four cycles. Afterward, the electrodes were soaked in deionized water for 1 h to exchange the residual ions contained within the electrodes. Subsequently, the electrodes were dried at 60 °C for 12 h in a vacuum oven. The average deposition mass of CoS on GE/NF substrate was ~ 0.4 mg. The involved electrochemical deposition process can be described by the following equations:

$$2H_2O + 2e^- \rightarrow 2OH^- + H_2 \quad (1)$$

$$SC(NH_2)_2 + 2OH^- \rightarrow S^{2-} + OC(NH_2)_2 + H_2O \quad (2)$$

$$Co^{2+} + S^{2-} \rightarrow CoS \quad (3)$$

Deposition of PPY film on 3D CoS/GE/NF electrode

Typically, 0.208 g p-TSA was firstly dissolved in 30 mL anhydrous alcohol. After vigorous stirring, 0.024 M pyrrole monomer was added into the aforementioned solution and stirred for 10 min to form a uniform solution (denoted as solution A). Meanwhile, 0.06 g APS was dissolved in 20 mL deionized water under stirring to form a uniform solution (denoted as solution B). Then, the as-prepared 3D CoS/

GE/NF electrode was placed in a clean petri dish. Solution A was slowly dropped into the sample by using a Transferpette to ensure the sample was just infiltrated (140 μL of solution A for each sample). Next, the same volume of solution B was dropped onto each sample. Afterwards, the samples were left in the dark for 24 h before rinsing with deionized water to remove residues. Finally, the product was dried at 60 °C overnight in a vacuum oven. By weighing the mass of the electrode before and after PPY deposition, the mass of the PPY film was measured to be 0.15 mg cm^{-2}.

Measurement and electrochemical characteristic

The crystal structure of the as-prepared samples was investigated by a powder X-ray diffractometer (XRD, D/max-2400, Dikagu, Japan) with radiation of Cu target (Kα, $\lambda = 0.1541$). Morphologies of the samples were observed by a field emission scanning electron microscopy (FESEM; JSM-6701, JOEL) and a high-resolution transmission electron microscopy (HRTEM; JEM 2010F, JOEL). Fourier-transform infrared (FT-IR) spectra of the samples were recorded by IFS66V/S spectrometer using pressed KBr pellets technique. The chemical surface state of the samples was characterized by X-ray photoelectron spectroscopy (XPS, Kratos AXIS Ultra DLD, Al Kα).

Electrochemical performance of all prepared samples was investigated on the aforementioned electrochemical working station within a three-electrode cell containing 1 M KOH electrolyte. Cyclic voltammetry (CV) and galvanostatic charge/discharge (GCD) techniques were used to evaluate the electrochemical performance of the prepared electrodes. Electrochemical impedance spectroscopy (EIS) measurements were performed by applying AC voltage with amplitude of 5 mV in a frequency range from 0.01 Hz to 100 kHz at open circuit potential. The specific capacitance (F g^{-1}) of the electrode was calculated based on the total mass of the electroactive materials (CoS and PPY) by using the equation as follows: $C = I \cdot \Delta t / \Delta V \cdot m$, where I, Δt, m, and ΔV are discharge current (A), discharge time (s), mass of electroactive materials (g), and the discharge voltage (V), respectively.

Results and discussion

Deposition of cobalt sulfide on NF and NF/GE substrates was performed through a simple electrodeposition method in a three-electrode-cell configuration at room temperature. The crystal structure of the as-prepared cobalt sulfide was determined by XRD technique. Considering the strong signal of NF substrate and its strong signal shield effect on the host material, the cobalt sulfide was electrochemically deposited on carbon cloth (CC) for XRD measurement. As observed in Fig. 1, besides a sharp peak at ~ 26° and a broad weak peak at

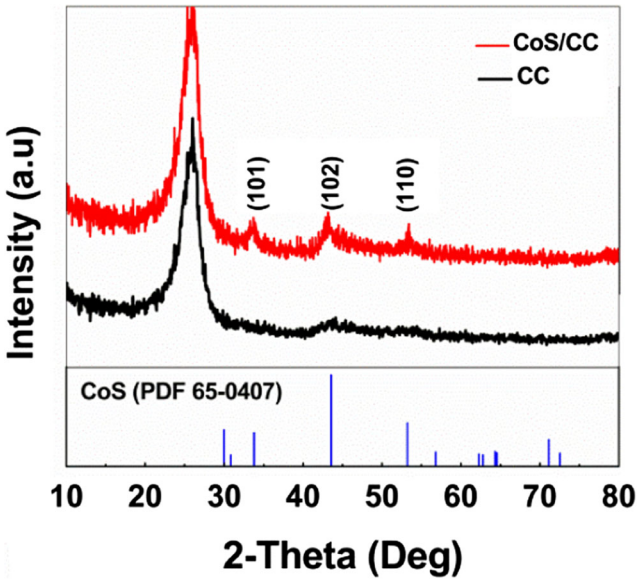

Fig. 1 XRD pattern of the PPY/CoS on carbon cloth substrate

~ 43° that originated from CC substrate, several diffraction peaks at 33.8°, 43.6°, and 53.2°, which matches well with the (101), (102), and (110) faces of hexagonal CoS (JCPDS card No. 65-0407), were also clearly detected. The survey XPS spectrum demonstrates the presence of Co and S on the surface of the as-prepared 3D CoS/GE/NF electrode (Fig. 2a) besides the physically adsorbed C and O elements. The core-level spectra of Co 2p and S 2p of the 3D CoS/GE/NF electrode are shown in Fig. 2b and c. The core-level spectra of Co2p can be fitted as two spin-orbit doublets and two shakeup satellites. The strong broad excitation satellite peak at 786.6 eV indicates a dominant proportion of Co(II) in the prepared Co-based composite. The difference of the binding energy between Co $2p_{1/2}$ and Co $2p_{3/2}$ is more than 15 eV, suggesting the co-existence of Co(II) and Co(III) in the composite electrode [27–31]. Figure 2c presents the core-level spectrum of S 2p region. The binding energy at 163.5 and 162.1 eV corresponds to the S $2p_{1/2}$ and S $2p_{3/2}$, respectively, suggesting that the S species exist as S^{2-} in composite electrode [32]. The satellite peaks at around 166–171 eV can be ascribed to the inconsequential amount of Co_xS_y ($x = 1, 2 \ldots 4$; $y = 1, 2 \ldots 9$) compounds, implying that there are small amount of nonstoichiometric cobalt sulfides existing in the electrodeposited CoS film [29]. Generally, by considering the XRD and XPS results, it can be claimed that the electrochemically deposited cobalt sulfide compound is dominantly composed of hexagonal structured CoS phase.

To tailor the interfacial contact between the active material and current collector, in present study, we deposit the CoS on both NF and GE/NF composite substrates, and investigate the effect of electrical contact on the electrochemical performance of CoS material. Graphene film was grown on NF matrix via a self-catalytic thermal CVD process. According to our

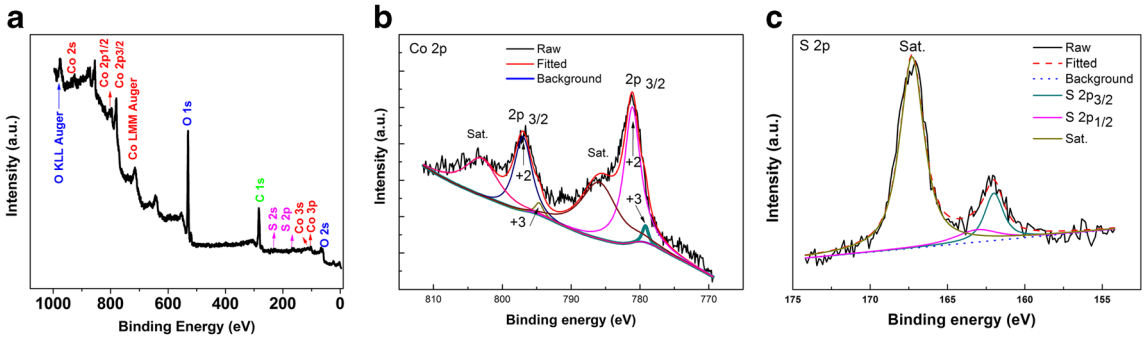

Fig. 2 **a** Survey XPS spectrum and **b** and **c** the core-level spectra of Co 2p and S 2p on 3D CoS/GE/NF electrode

previous reports, the grown graphene film consists of single- to few-layer graphene, forming a uniform 3D GE/NF matrix for depositing electroactive host materials [26]. Figure 3 shows the FESEM images of the electrodeposited CoS on GE/NF and NF matrices. As observed in inset of Fig. 3a, after electrochemical process, CoS film is uniformly deposited on the skeleton of GE/NF matrix. No obvious aggregation of CoS nanoparticles is observed. Higher-magnification FESEM image (Fig. 3b) suggests that the electrodeposited CoS film actually is composed of numerous cross-linked CoS nanosheets with thickness of ~ 30 nm, demonstrating a typical porous morphology feature. HRTEM image further confirms the highly porous structure of CoS film prepared in our study (Fig. 3c). The electrodeposited CoS on pristine NF matrix is roughly same as that on GE/NF matrix. The similar morphology of CoS on two matrices enables us to investigate the effect of interfacial electrical contact on the electrochemical performance of CoS material.

The electrochemical behavior of CoS on NF and GE/NF matrices was investigated by CV and GCD techniques. Figure 4a shows the CV curves of CoS/NF electrode at various scan rates. Obviously, all CV curves is characterized by a pair of well-defined redox peaks within a low potential window of −0.1~0.02 V (P_1/P_2 couple) and a pair of highly symmetric redox peaks within a higher potential window of 0.05~0.45 V (P_3/P_4 couple). While for 3D CoS/GE/NF electrode, the CV curves at different scan rates are dominated by the P_3/P_4 redox couple (Fig. 4b). The P_1/P_2 redox couple was suppressed due to the strong current peak of the P_3/P_4 redox couple. By comparison, the current density of the P_3/P_4 couple in the CV curves of 3D CoS/GE/NF electrode is nearly twice that of CoS/NF electrode at the same scan rate, suggesting the enhanced *I-V* response of 3D CoS/GE/NF electrode due to the deposition of graphene film. The performance difference of the two electrodes also can be reflected by their discharge curves. As shown in Fig. 4c, the discharge curves of CoS/NF at 1 A g^{-1} consist of a remarkable inflection point at ~0.2 V and a faint inflection point at −0.05 V, corresponding to the reduction of P_4 and P_2 peaks in CV curve. For 3D CoS/GE/NF electrode, its discharge curve is characterized by an obvious inflection point at ~0.2 V (Fig. 4d). According to their discharge curves, the specific pseudocapacitances of two electrodes at various current densities are calculated and are plotted in Fig. 4e. The 3D CoS/GE/NF electrode can deliver the high pseudocapacitance of 2308, 2088, 1932, 1813, 1710, and 1627 F g^{-1} at current densities of 1, 3, 5, 10, 15, and 20 A g^{-1}, giving a high capacitance retention of 70.49% within the presented current density range in our experiment. It should be noted that the gravimetric fraction of the GE foam in our study cannot be precisely measured because of its ultra-thin layer (less than five graphene layers, <0.02 mg cm^{-2}). Meanwhile, considering the extremely low pseudocapacitance value of CVD-graphene (< 250 F g^{-1} at 1 A g^{-1}), the pseudocapacitance contribution of GE foam to the whole electrode can therefore be fully ignored. For CoS/NF electrode, it delivers the relatively lower pseudocapacitance values than that of 3D CoS/GE/NF electrode at same current density. For example, at 1 A g^{-1}, only a low pseudocapacitance value of 1272 F g^{-1} can be achieved for CoS/NF electrode, which value is even much lower than that of 3D CoS/GE/NF electrode at 20 A g^{-1}. It can be inferred that enhanced

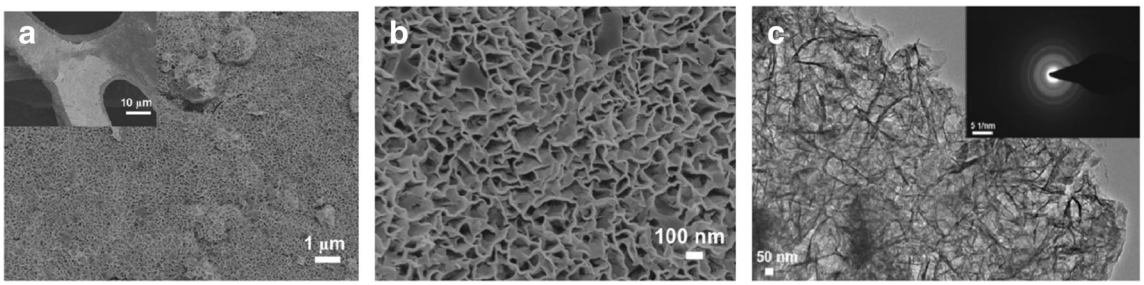

Fig. 3 FESEM images of CoS nanoflakes deposited on **a** GE/NF substrate and **b** NF substrate. **c** HRTEM image of CoS on 3D CoS/GE/NF electrode

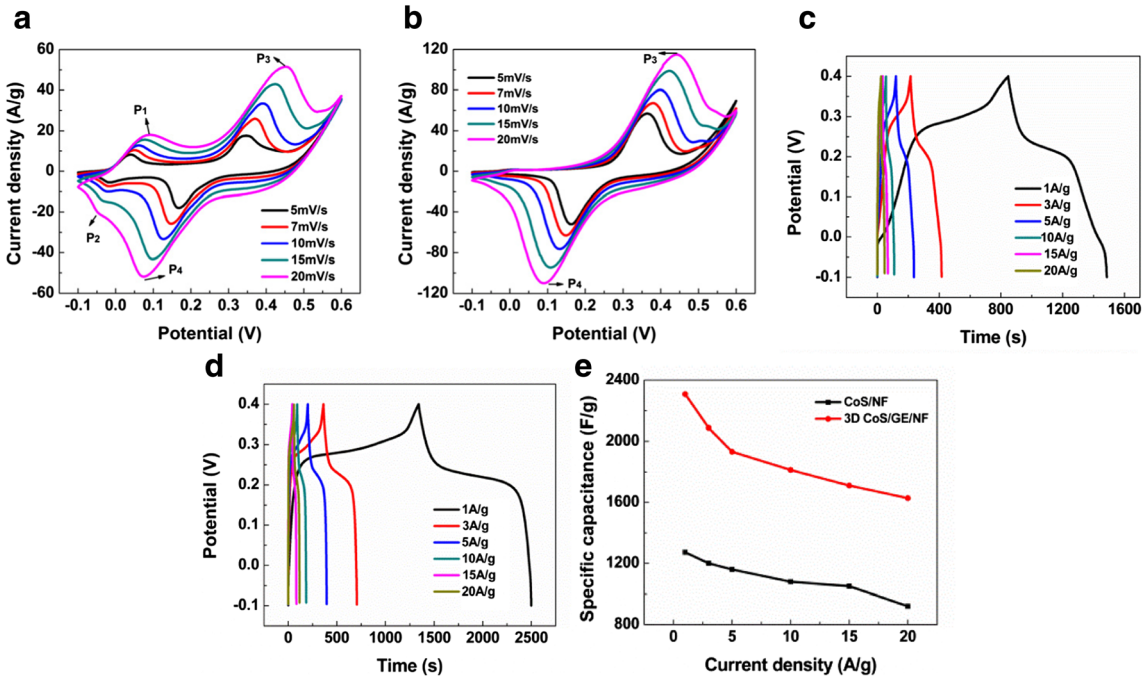

Fig. 4 CV curves of **a** CoS/NF and **b** 3D CoS/GE/NF electrodes. GCD curves of **c** CoS/NF and **d** 3D CoS/GE/NF electrodes. **e** Specific capacitance of CoS/NF and 3D CoS/GE/NF electrodes

pseudocapacitive performance of CoS on GE/NF current collector is possibly related to the graphene film in improving the electrical contact between the active material and current collector. This can be verified by the great decline of the charge-transfer resistance and equivalent series resistance of the 3D CoS/GE/NF electrode as compared to that of 3D CoS/NF electrode, as shown in Fig. 6f. Although the presence of the graphene greatly improves the pseudocapacitance value of the CoS, the cycling performance of CoS on GE/NF still does not satisfy the practical requirement of high-performance energy storage device. As can be seen from Fig. 6e, after 1000 cycles, only 26% of the capacitance retention is remained. Therefore, more efforts should be devoted to further improving the cycling stability of CoS/GE/NF electrode.

Deposition of highly conductive polymer coating is an alternative strategy to boost the electrochemical performance of the active material and consolidate the integrity of the whole electrode. In present study, PPY, a kind of highly conductive polymer, was selected and deposited on 3D CoS/GE/NF electrode through a polymerization strategy to improve the electrochemical performance of the CoS material and stabilize the geometry configuration of the electrode. After the polymerization process, a thin layer of cross-linked PPY network is coated on 3D CoS/GE/NF electrode (Fig. 5a), preserving the porous surface morphology of the CoS nanosheets on GE/NF current collector. Figure 5b shows the FT-IR spectrum of PPY/CoS composite. Compared with that of CoS, several new characteristic peaks can be found in the FT-IR spectrum of PPY/CoS composite powder. The peak at 1546 cm^{-1} is assigned to the pyrrole ring, i.e., the combination of C=C and C–C stretching vibrations. The band at 1456 cm^{-1} corresponds to C–N stretching vibration [33]. The peak at 1038 cm^{-1} can be ascribed to the C–H deformation vibration [34]. The existence of PPY film on the surface of CoS can be further confirmed by the XPS spectra of 3D PPY/CoS/GE/NF electrode, as shown in Fig. 5c. It can be seen that the deposited film consists of C, S, O, Co, and N elements. In N 1s spectrum (Fig. 5d), the two deconvoluted peaks centered at 397.8 and 399.7 eV can be assigned to the neutral imine-like structured –C=N– group and neutral amine-like structured –NH– group, respectively [35, 36]. The NH^+ group (~400.8 eV) reported in literature is very weak in our study. All these together confirm the deposition of PPY film and successful preparation of porous 3D PPY/CoS/GE/NF electrode.

Figure 6 shows the electrochemical performance of the 3D PPY/CoS/GE/NF electrode. For comparison, the electrochemical performance of 3D PPY/GE/NF and 3D CoS/GE/NF electrodes were also tested. As can be seen from the normalized CV curves of the three electrodes at 5 mV s^{-1} (Fig. 6a), the pure PPY electrode exhibits extremely low and negligible electric current. Compared with that of 3D CoS/GE/NF electrode, the 3D PPY/CoS/GE/NF electrode shows similar CV curve but enormously enhanced *I-V* response (Fig. 6a). At scan rates of 5-20 mV s^{-1}, the peak current densities of the 3D PPY/CoS/GE/NF electrode augment with the square root of the scan rate (Fig. 6b). This implies that the deposition of the PPY network does not prevent the intimate contact between the CoS and electrolyte. According to the discharge curves as shown in Fig. 6c, after depositing PPY film, the electrodeposited 3D CoS can deliver the high pseudocapacitance values of 3450,

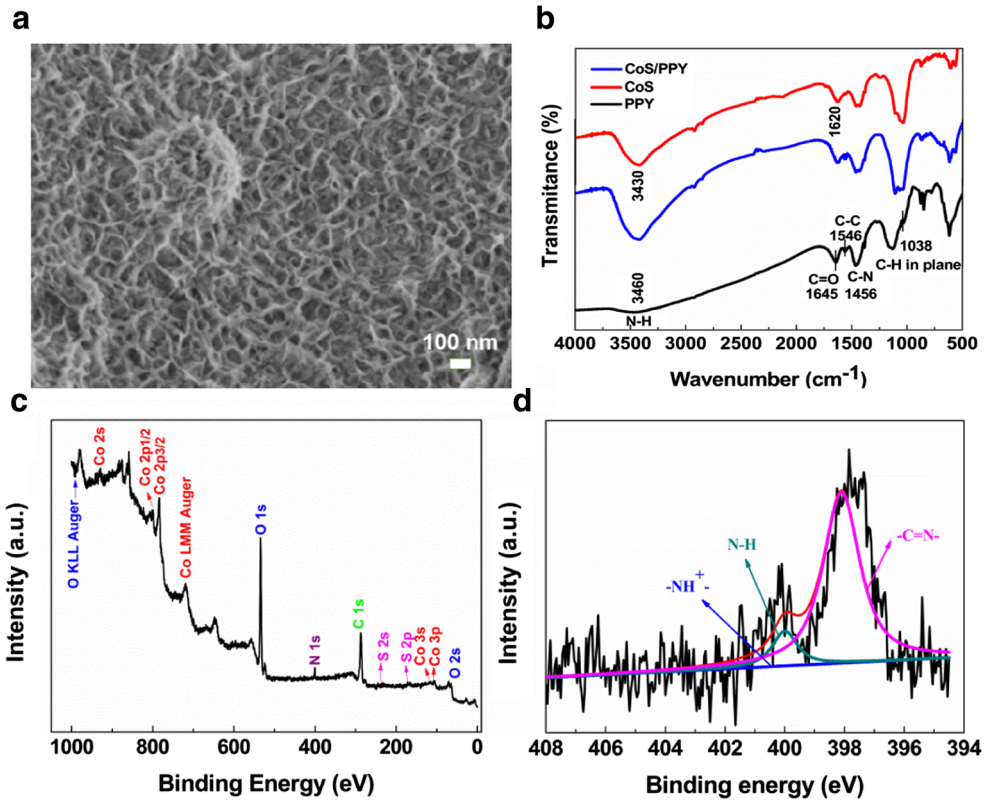

Fig. 5 **a** FESEM image of 3D PPY/CoS/GE/NF electrode. **b** FT-IR spectra of CoS, PPY, and CoS/PPY composite. **c** Survey XPS spectrum and **d** N 1s core-level spectrum of 3D PPY/CoS/GE/NF electrode

3138, 2813, 2728, 2340, and 2160 F g^{-1} at current densities of 1, 3, 5, 10, 15, and 20 A g^{-1}, respectively, much higher than that of 3D PPY/GE/NF electrode and 3D CoS/GE/NF at same current density (Fig. 6d). Even including the mass of PPY film which has the extremely low pseudocapacitance value of 260 and 95 F g^{-1} at current densities of 1 and 20 A g^{-1}, the specific pseudocapacitance values of 3D PPY/CoS/GE/NF are much higher than those of 3D CoS/GE/NF, especially at the current

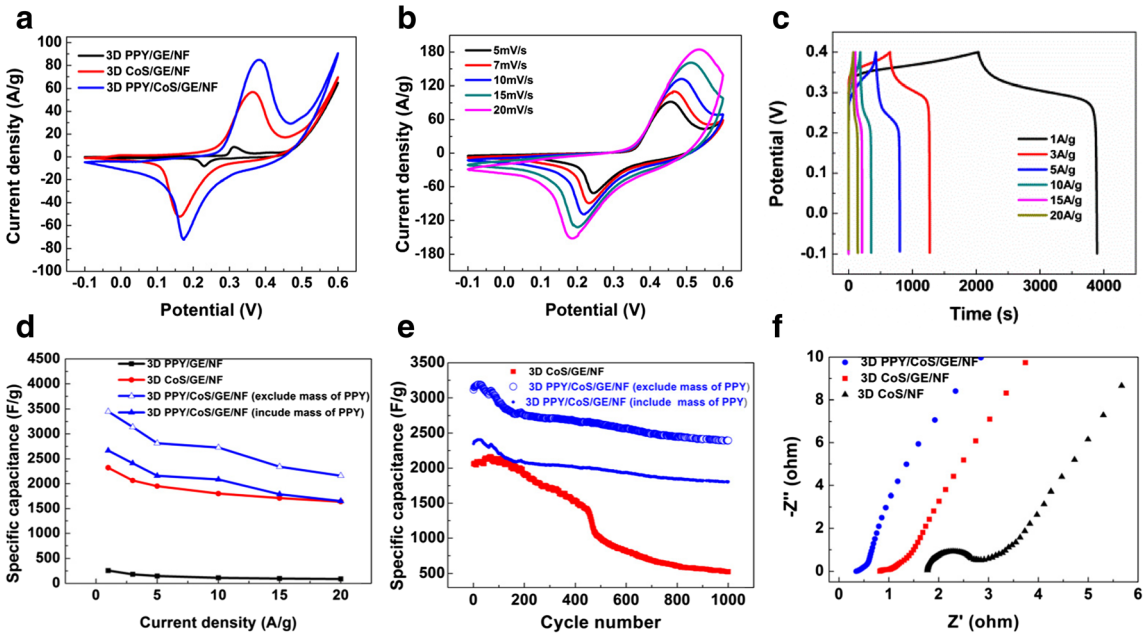

Fig. 6 Electrochemical performances of 3D PPY/CoS/GE/NF and 3D CoS/GE/NF electrodes. **a** Comparative CV curves of two electrodes at a scan rate of 5 mV s^{-1}. **b** CV curves of 3D PPY/CoS/GE/NF electrode at various scan rates. **c** Charge-discharge curves of 3D PPY/CoS/GE/NF electrode at various current densities. **d** Specific capacitances of the two electrodes at different current densities. **e** Cycling performance of the two electrodes at 3 A g^{-1}. **f** Nyquist plots of the EIS spectra of the two electrodes

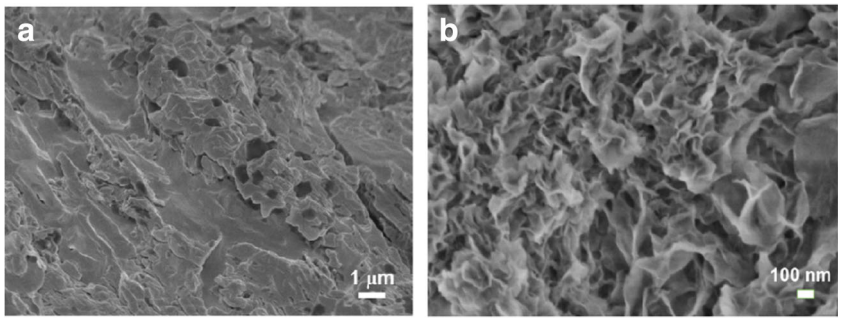

Fig. 7 FESEM images of the two electrodes after 1000 cycles. **a** 3D CoS/GE/NF and **b** 3D PPY/CoS/GE/NF electrodes

densities of 1, 3, 5, and 10 A g^{-1}. The enormous enhanced capacitance value of 3D PPY/CoS/GE/NF electrode over 3D CoS/GE/NF electrode is closely related to the presence of porous PPY film on electrode surface which greatly improves the electrical conductivity of the whole electrodes and thus decreases the equivalent series resistance of the 3D PPY/CoS/GE/NF-based three-electrode-cell system. This can be validated by the EIS spectra of 3D PPY/CoS/GE/NF electrode (Fig. 6f), in which smaller intercept of the semicircle on the real axis was observed. Besides the significant role of the PPY network in improving the pesudocapacitance values of the CoS material, the presence of PPY coating also can improve the cycling stability of the electrode. As observed in Fig. 6e, after 1000 cycles, the 3D PPY/CoS/GE/NF electrode can give a capacitance retention of 73%, much higher than 26% capacitance retention of 3D CoS/GE/NF electrode. More importantly, the capacitance of 3D PPY/CoS/GE/NF electrode at 1000th cycle still is comparable to that of 3D CoS/GE/NF electrode at 1st cycle, further confirming the significant role of PPY film in improving the cycling stability of the CoS material.

The significant role of PPY in consolidating the integrity and improving the cycling stability of the electrode can be verified by the FESEM image of the electrode after cycling test. As demonstrated in Fig. 7a, the 3D CoS/GE/NF electrode hardly maintains its nanosheet structure and evolved into a flatten surface after cycling test, while the 3D PPY/CoS/GE/NF electrode (Fig. 7b) roughly preserves its initial surface morphology as shown in Fig. 5a. The enormous difference of surface morphology of the two electrodes after cycling further validates the important role of PPY in improving the integrity and cycling stability of the electrode.

Conclusions

We have successfully synthesized the CoS materials on 3D GE/NF and NF substrates through an electrochemical deposition method. Owing to the significant role of graphene in improving the interfacial electrical contact between the electroactive material and current collector, the electrochemical performance of CoS was greatly improved. The electrodeposited 3D CoS on GE/NF current collector delivered much higher specific capacitance value and comparable rate capability as compared with those of 3D CoS deposited on NF current collector. The deposition of PPY porous film on 3D CoS/GE/NF electrode can further enhance the electrochemical performance of CoS material due to the advantage of PPY film in improving the electrical conductivity of the electrode and reinforcing the integrity of the whole electrode. As a result, the PPY-coated 3D CoS material exhibits higher specific capacitance (3450 F g^{-1} at 1 A g^{-1}), better rate capability (62.61% at 20 A g^{-1}), and higher capacitance retention (73% at 3 A g^{-1} after 1000 cycles) over those of 3D CoS on GE/NF current collector.

Funding information Dr. Li thanks for the partial financial support by the State Key Laboratory of Advanced Processing and Recycling of Nonferrous Metals (No. SKLAB02014002, Lanzhou University of Technology), and Dr. Wan thanks for the partial financial support by the Western Doctoral program of the Chinese Academy of Sciences.

References

1. Kanan MW, Nocera DG (2008) In situ formation of an oxygen-evolving catalyst in neutral water containing phosphate and Co^{2+}. Science 321(5892):1072–1075. https://doi.org/10.1126/science.1162018
2. Zeng W, Zhang G, Wu X, Zhang K, Zhang H, Hou S, Li C, Wang T, Duan H (2015) Construction of hierarchical CoS nanowire@$NiCo_2S_4$ nanosheet arrays via one-step ion exchange for high-performance supercapacitors. J Mater Chem A 3(47):24033–24040. https://doi.org/10.1039/C5TA05934H
3. Dong J, Wang Z, Kang X (2016) The synthesis of graphene/PVDF composite binder and its application in high performance MnO_2 supercapacitors. Colloids Surf A Physicochem Eng Asp 489:282–288. https://doi.org/10.1016/j.colsurfa.2015.10.060
4. Kim GM, Park JH, Lee JW (2016) Formation of hollow Co_3O_4 nanoparticles on nitrogen–doped porous carbons for highly capacitive performance. Chemistryselect 1(3):560–566. https://doi.org/10.1002/slct.201600112
5. Zhang X, Zeng X, Yang M, Qi Y (2014) Investigation of branch-like MoO_3/polypyrrole hybrid with enhanced electrochemical performance used as electrode in supercapacitors. Acs Appl Mater Inter 6(2):1125–1130. https://doi.org/10.1021/am404724u
6. CC H, Chang KH, Mingchamp Lin A, YT W (2006) Design and tailoring of the nanotubular arrayed architecture of hydrous RuO_2 for next generation supercapacitors. Nano Lett 6:2690–2695
7. Wu Y, Liu S, Zhao K, He Z, Yuan H, Lv K, Jia G (2016) Chemical deposition of MnO_2 nanosheets on graphene-carbon nanofiber

paper as free-standing and flexible electrode for supercapacitors. Ionics 22(7):1185–1195. https://doi.org/10.1007/s11581-015-1625-6
8. Yuan C, Zhang X, Su L, Gao B, Shen L (2009) Facile synthesis and self-assembly of hierarchical porous NiO nano/micro spherical superstructures for high performance supercapacitors. J Mater Chem 19(32):5772–5777. https://doi.org/10.1039/b902221j
9. Yan J, Fan Z, Wei S, Ning G, Tong W, Qiang Z, Zhang R, Zhi L, Fei W (2012) Advanced asymmetric supercapacitors based on $Ni(OH)_2$/graphene and porous graphene electrodes with high energy density. Adv Funct Mater 22(12):2632–2641. https://doi.org/10.1002/adfm.201102839
10. Liu J, Jiang J, Cheng C, Li H, Zhang J, Gong H, Fan HJ (2011) Co_3O_4 nanowire@MnO_2 ultrathin nanosheet core/shell arrays: a new class of high-performance pseudocapacitive materials. Adv Mater 23(18):2076–2081. https://doi.org/10.1002/adma.201100058
11. Mu J, Chen B, Guo Z, Zhang M, Zhang Z, Zhang P, Shao C, Liu Y (2011) Highly dispersed Fe_3O_4 nanosheets on one-dimensional carbon nanofibers: synthesis, formation mechanism, and electrochemical performance as supercapacitor electrode materials. Nano 3:5034–5040
12. Bai Y, Liu M, Sun J, Gao L (2016) Fabrication of Ni-Co binary oxide/reduced graphene oxide composite with high capacitance and cyclicity as efficient electrode for supercapacitors. Ionics 22(4):535–544. https://doi.org/10.1007/s11581-015-1576-y
13. Huang J, Lei T, Wei X, Liu X, Liu T, Cao D, Yin J, Wang G (2013) Effect of Al-doped β-$Ni(OH)_2$ nanosheets on electrochemical behaviors for high performance supercapacitor application. J Power Sources 232:370–375. https://doi.org/10.1016/j.jpowsour.2013.01.081
14. Zhang Y, Wang J, Ye J, Wan P, Wei H, Zhao S, Li T, Hussain S (2016) $NiCo_2O_4$ arrays nanostructures on nickel foam: morphology control and application for pseudocapacitors. Ceram Int 42(13):14976–14983. https://doi.org/10.1016/j.ceramint.2016.06.142
15. JM X, Ma KY, Cheng JP (2015) Controllable in situ synthesis of $Ni(OH)_2$ and NiO films on nickel foam as additive-free electrodes for electrochemical capacitors. J Alloys Compd 653:88–94
16. Yang J, Liu H, Martens WN, Frost RL (2010) Synthesis and characterization of cobalt hydroxide, cobalt oxyhydroxide, and cobalt oxide nanodiscs. J Phys Chem C 87:923–937
17. Mehrabad JT, Aghazadeh M, Maragheh MG, Ganjali MR, Norouzi P (2016) α-$Co(OH)_2$ nanoplates with excellent supercapacitive performance: electrochemical preparation and characterization. Mater Lett 184:223–226. https://doi.org/10.1016/j.matlet.2016.08.069
18. Xia X, Zhu C, Luo J, Zeng Z, Guan C, Ng CF, Zhang H, Fan HJ (2014) Synthesis of free-standing metal sulfide nanoarrays via anion exchange reaction and their electrochemical energy storage application. Small 10(4):766–773. https://doi.org/10.1002/smll.201302224
19. Zhai S-Y, Li L-L, Wang M-G (2017) A facile synthesis about amorphous CoS2 combined with first principle analysis for supercapacitor materials. Ionics 23(7):1819–1830. https://doi.org/10.1007/s11581-017-1991-3
20. Jiang Z, Lu W, Li Z, Ho KH, Li X, Jiao X, Chen D (2014) Synthesis of amorphous cobalt sulfide polyhedral nanocages for high performance supercapacitors. J Mater Chem A 2(23):8603–8606. https://doi.org/10.1039/C3TA14430E
21. Lin JY, Chou SW (2013) Cathodic deposition of interlaced nanosheet-like cobalt sulfide films for high-performance supercapacitors. RSC Adv 3(6):2043–2048. https://doi.org/10.1039/C2RA22373B
22. Liu B, Kong D, Zhang J, Wang Y, Chen T, Cheng C, Yang H (2016) 3D hierarchical Co_3O_4@Co_3S_4 nanoarrays as cathode materials for asymmetric pseudocapacitor. J Mater Chem A 4(9):3287–3296. https://doi.org/10.1039/C5TA09344A
23. Xie J, Liu S, Cao G, Zhu T, Zhao X (2013) Self-assembly of CoS_2 /graphene nanoarchitecture by a facile one-pot route and its improved electrochemical Li-storage properties. Nano Energy 2(1):49–56. https://doi.org/10.1016/j.nanoen.2012.07.010
24. Zhou YX, Yao HB, Wang Y, Liu HL, Gao MR, Shen PK, SH Y (2010) Hierarchical hollow Co_9S_8 microspheres: solvothermal synthesis, magnetic, electrochemical, and electrocatalytic properties. Chem Eur J 16(39):12000–12007. https://doi.org/10.1002/chem.200903263
25. Wang Q, Jiao L, Han Y, Du H, Peng W, Huan Q, Song D, Si Y, Wang Y, Yuan H (2011) CoS_2 hollow spheres: fabrication and their application in lithium-ion batteries. J Phys Chem C 115(16):8300–8304. https://doi.org/10.1021/jp111626a
26. Wang L, Li X, Guo T, Yan X, Tay BK (2014) Three-dimensional $Ni(OH)_2$ nanoflakes/graphene/nickel foam electrode with high rate capability for supercapacitor applications. Int J Hydrog Energy 39(15):7876–7884. https://doi.org/10.1016/j.ijhydene.2014.03.067
27. Shi J, Li X, He G, Zhang L, Li M (2015) Electrodeposition of high-capacitance 3D CoS/graphene nanosheets on nickel foam for high-performance aqueous asymmetric supercapacitors. J Mater Chem A 3(41):20619–20626. https://doi.org/10.1039/C5TA04464B
28. Meng X, Deng J, Zhu J, Bi H, Kan E, Wang X (2016) Cobalt sulfide/graphene composite hydrogel as electrode for high-performance pseudocapacitors. Sci Rep 6(2016)
29. Das S, Sudhagar P, Nagarajan S, Ito E, Sang YL, Kang YS, Choi W (2012) Synthesis of graphene-CoS electro-catalytic electrodes for dye sensitized solar cells. Carbon 50(13):4815–4821. https://doi.org/10.1016/j.carbon.2012.06.006
30. Galtayries A, Grimblot J (1999) Formation and electronic properties of oxide and sulphide films of Co, Ni and Mo studied by XPS. J Electron Spectrosc Relat Phenom s 98–99:267–275
31. Yan M, Yao Y, Wen J, Lu L, Kong M, Zhang G, Liao X, Yin G, Huang Z (2016) Construction of a hierarchical $NiCo_2S_4$@PPy core–shell heterostructure nanotube array on Ni foam for a high-performance asymmetric supercapacitor. Acs Appl Mater Inter 8(37):24525–24535. https://doi.org/10.1021/acsami.6b05618
32. Lin JY, Liao JH (2012) Mesoporous electrodeposited-CoS film as a counter electrode catalyst in dye-sensitized solar cells. J Electrochem Soc 159(2):D65–D71. https://doi.org/10.1149/2.036202jes
33. Yang C, Wang T, Liu P, Shi H, Xue D (2009) Preparation of well-defined blackberry-like polypyrrole/fly ash composite microspheres and their electrical conductivity and magnetic properties. Curr Opin Solid State Mater Sci 13(5-6):112–118. https://doi.org/10.1016/j.cossms.2009.06.002
34. Yang X, Li L (2010) Polypyrrole nanofibers synthesized via reactive template approach and their NH_3 gas sensitivity. Synth Met 160(11-12):1365–1367. https://doi.org/10.1016/j.synthmet.2010.04.015
35. Lei J, Cai Z, Martin CR (1992) Effect of reagent concentrations used to synthesize polypyrrole on the chemical characteristics and optical and electronic properties of the resulting polymer. Synth Met 46(1):53–69. https://doi.org/10.1016/0379-6779(92)90318-D
36. Zhou H, Han G, Xiao Y, Chang Y, Zhai HJ (2014) Facile preparation of polypyrrole/graphene oxide nanocomposites with large areal capacitance using electrochemical codeposition for supercapacitors. J Power Sources 263:259–267. https://doi.org/10.1016/j.jpowsour.2014.04.039